# Constitutive Models for Concrete in Plasticity

**Ansari Abu Usama[1] M. G. Shaikh[2]**
[1]Student [2]Associate Professor
[1,2]Department of Applied Mechanics
[1,2]Government Engineering College Aurangabad

*Abstract*— For a structural engineer, the appropriate success in analysis and design of concrete structures depends on his/ her understanding of the proper behavior of the concrete material under different loading conditions. Therefore in this work the behavior of concrete under different loading conditions is studied. Litewka et. al. (2002) plasticity model available in literature is studied to obtain realistic results. Yield function, hardening and softening function, plastic potential function, flow rule etc. are required to define plasticity model. The material behavior described by this plasticity model is compared with experimental data. Model performance shows predicted results are in good agreement with the experimental data. Depending upon accuracy in material behavior prediction, the corresponding computational models will be very useful in development of commercial software for analysis and design of concrete structure.

***Key words:*** Concrete, Plasticity, Constitutive Modeling, Compression

## I. INTRODUCTION

Concrete is a heterogeneous, cohesive-frictional material and exhibits complex non-linear inelastic behavior under multi-axial stress states. The increased use of concrete as primary structural material in building complex structures such as reactor vessels, dams, offshore structures, etc., necessitates the development of sophisticated material models for accurate prediction of the material response to a variety of loading situations. The new developments which are taking place in the area of concrete technology resulted in new generation of concretes, which are better in terms of performance, such as high strength concrete (HSC) , reactive powder concrete (RPC), high performance light weight concrete (HPLC) and self-compacting concrete, etc. further stressed the need for new material models.

Concrete structures are often analyzed by means of the finite element method. Analysis of a structural engineering problem by finite element method is based on solution of a set of equilibrium equations and a kinematically admissible displacement field. These are supplemented by boundary and initial conditions of a particular problem. These statically and kinematically admissible sets are independent of each other, and to link them material constitutive relations are required [1].

The incremental theory of plasticity has been widely applied to describe the inelastic behavior of engineering materials such as metals, concrete and soils. There are three basic assumptions in this theory [3].

1) The existence of an initial yield surface in stress space that defines the stress level at which plastic deformation begins.
2) A hardening rule that defines the change of the loading surface as well as the change of the hardening properties of the material during the course of plastic flow.
3) A flow rule that is related to a plastic potential function and gives an incremental plastic stress-strain relation.

The objective of this work is to study the behavior of concrete under different loading conditions proposed by many researchers as described in section II and compared with experimental results of Kupfer [4].

## II. LITERATURE SURVEY

The various plasticity models proposed by different authors are as follows:

Han and Chen (1985) attempted to develop a relatively comprehensive and sophisticated plasticity model to represent adequately the important features of inelastic deformational behavior of concrete, including brittle cracking in tension, work-hardening and quasi-ductile behavior in compression, hydrostatic pressure sensitivities, and nonlinear volume dilatancy [3]. The model is

$$d\sigma_{ij} = (C^e_{ijkl} + C^p_{ijkl})d\varepsilon_{kl} \qquad (2.1)$$

Where
$C^e_{ijkl}$ Elastic stiffness tensor
$C^p_{ijkl}$ Plastic stiffness tensor

Comparisons of the model predictions have been performed with two sets of test results. The well-known Kupfer's test [4] was considered first, which provide stress-strain behaviors of concrete under biaxial loadings. The second set of test data was taken from the report of Air Force Weapon's Laboratory presented by Traina, Babcock and Schreyer.

It is observed that for a plasticity constitutive model, the failure surface serves as a bounding surface, representing the multiaxial strength of the material. The model which assumes a closed yield surface and uses a non uniform hardening rule as well as a nonassociated flow rule, has been shown to produce results in good agreement with experimental data for a wide range of stress states and different types of concrete material. It is also found model capable of representing the important characteristics of concrete behavior, including brittle failure in tension, ductile behavior in compression, pressure sensitivity, and volumetric dilatation under compressive loadings.

Han and Chen (1987) used the plasticity theory, including the concepts of plastic-fracturing theory to model the nonlinear multiaxial strain hardening- softening behavior [5]. The primary objective of the research was to develop a relatively comprehensive and sophisticated constitutive model for progressive failure analysis of concrete structures. The incremental elastic-plastic constitutive relation is

$$d\sigma_{ij} = \left(c^e_{ijkl} - \frac{1}{h}c^e_{ijmn}\frac{\partial g}{\partial \sigma_{mn}}\frac{\partial f}{\partial \sigma_{pq}}c^e_{pqkl}\right)d\epsilon_{kl} \qquad (2.2)$$

Where
$C^e_{ijkl}$ Elastic stiffness tensor
h= a scalar

 

f= Loading function
g= Plastic potential function

Model prediction was compared with the test data of AFWL for low-strength concrete reported by Traina, et al. Further comparisons were made, and the results show that the model is in good agreement with experimental results involving a wide range of stress states.

Author has verified in an extensive comparison with a wide range of available experimental results. The strain-softening model, using the volumetric strain as the loading criterion, works well in biaxial and triaxial compressive loadings with a relatively low hydrostatic compressive stress.

Hsuan and William (1989) used the elastic strain-hardening plastic model because it was more general and more accurate than the earlier elastic-perfectly plastic models; to develop a non-associated plasticity model for concrete [6].Incremental plastic stress-strain relations based on the flow is expressed as

$$d(\sigma) = [c]_{ep} d(\varepsilon) = ([c]_e - [c]_p) d(\varepsilon) \quad (2.3)$$

Where

$$[c]_p = \frac{[c]_e \frac{\partial G}{\partial \sigma} \frac{\partial F}{\partial \sigma} [c]_e}{H \frac{G}{\bar{\sigma}} + \frac{\partial F}{\partial \sigma} [c]_e \frac{\partial G}{\partial \sigma}} \quad (2.4)$$

H= Plastic hardening modulus.
$[c]_e$= Elastic stiffness tensor.
F= Loading function.
G= Plastic potential function.

This proposed elastic strain-hardening plastic model for plain concrete was tested and compered with the experimental data of Kupfer et al. (1969). In the numerical analysis, a nine-node Lagrangian shell element was employed, and a full Gaussian integration (3 X 3) rule was used for that element to avoid the possibility of any zero energy modes.

The author concluded that this material model is adequate in describing the plastic behavior of plain concrete. Further, it have been shown that the predictions based on the nonassociated flow rule show very good agreement with the test data, while the results achieved using an associated flow rule are poor, especially in regions of combined high compression with low tension.

Peter Grassl et al.(2002), used the theory of plasticity to model the behaviour of plain concrete subjected to multiaxial compressive loading [7]. The behavior of concrete in compression was characterized by inelastic deformations. Instead of the length of the plastic strain vector, the volumetric part was used as a hardening parameter. Author proposed a novel hardening law which is given by

$$\dot{k}(\dot{\varepsilon}^p) = \dot{\varepsilon}_v^p = \delta_{ij} \dot{\varepsilon}_{ij}^p = \dot{\lambda} \delta_{ij} \frac{\partial g}{\partial \sigma_{ij}} = \dot{\lambda} \frac{\sqrt{3}}{\sqrt{q(k)} f_c} \quad (2.5)$$

Where $\delta_{ij}$ is the Kronecker delta, $f_c$ compressive strength, $\dot{\lambda}$ plastic multiplier and g plastic potential function, $q(k)$ hardening function.

The response of the constitutive model was compared to experimental results from uniaxial, biaxial and triaxial compression tests.

The author concluded that the model predicts the load resistance and the deformation capacity of plain concrete in uniaxial, biaxial and triaxial compression by means of one calibration. Experimental results for strength and deformation behaviour were found to be in good agreement with the model prediction.

Andrzej Litewka et. al. (2002) studied experimentally the deformation and damage induced anisotropy of initially isotropic brittle material for uni-axially compressed concrete [8]. The aim of authors was to detect experimentally the existence of the deformation and damage-induced anisotropy of concrete. The second objective of this study was a formulation of the theoretical model based on continuum damage mechanics and on theory of tensor function representation. The generalized stress strain relations for anisotropic elastic solids

$$\varepsilon_{ij} = A_{ijkl} \sigma_{kl} \quad (2.6)$$

Where $\varepsilon_{ij}$ is the strain tensor, $\sigma_{kl}$ is the stress tensor and $A_{ijkl}$ is the material constants of orthotropically damaged solid

$$A_{ijkl} = -\frac{v_0}{E_0}\delta_{ij}\delta_{kl} + \frac{1+v_0}{E_0}(\delta_{ik}\delta_{jl} + \delta_{il}\delta_{jk}) + C(\delta_{ij}D_{kl} + D_{ij}\delta_{kl}) + D(\delta_{ik}D_{jl} + \delta_{jl}D_{ik} + \delta_{jk}D_{il}) \quad (2.7)$$

The above equation contains the Kronecker delta $\delta_{ij}$, the Young modulus $E_0$ and Poisson ratio $\nu_0$ for original undamaged material, two constants $C$ and $D$ to be determined experimentally and the second order symmetric damage effect tensor $D_{ij}$ responsible for current state of internal structure of the material.

The experimental stress-strain curves for the specimens of ordinary concrete C20 were compared with the theoretical predictions obtained from the mathematical model. Elastic constants obtained in experiments described in their work were compared with the theoretical results.

Experimental verification of the theoretical model performed by employing available experimental data for concrete subjected to multi-axial state of stress showed that theoretical stress-strain curves for bi-axial load coincide with experimental data. Less satisfactory agreement of experimental curves and theoretical predictions for three-axial state of stress was explained by usually large scatter of experimental results obtained for this type of loading.

Papanikolaou and Kappos (2007) presented confinement-sensitive plasticity constitutive model for concrete in triaxial compression, aiming to describe the strength and deformational behaviour of both normal and high-strength concrete under multiaxial compression [9]. In order to describe the concrete triaxial stress state during plastic flow, a three-parameter hydrostatic-pressure-sensitive loading surface was selected. . It was described by the following equation, in terms of Haigh–Westergaard coordinates

$$f(\xi,\rho,\theta) = \left(\sqrt{1.5}\frac{\rho}{k(\kappa)f_c}\right)^2 + m\left(\frac{\rho}{\sqrt{6}k(\kappa)f_c}r(\theta,e) + \frac{\xi}{\sqrt{3}k(\kappa)f_c}\right) - c(\kappa) = 0 \quad (2.8)$$

Where (m) friction parameter and the (r) elliptic function.
Hardening parameter is define as

$$k(\kappa) = k(\varepsilon_v^p) = k_0 + (1 -$$

 

$$k_0)\sqrt{1-\left(\frac{\varepsilon_{v,t}^{p}-\varepsilon_{v}^{p}}{\varepsilon_{v,t}^{p}}\right)^2} \qquad (2.9)$$

Where

$k_0 = \frac{\sigma_{c0}}{f_c}$

$\sigma_{c0}$= uniaxial concrete stress

$\varepsilon_{v,t}^{p}$= threshold value of plastic volumetric strain

$$\varepsilon_{v,t}^{p} = \frac{f_c}{E_c}(1-2v)$$

$\varepsilon_{v}^{p}$= plastic volumetric strain

The concrete constitutive model was implemented in a stand-alone software application, including a constitutive driver operating at the material stress‑strain level. Its performance was evaluated for both normal and high-strength concrete, by comparisons with uniaxial, biaxial and triaxial compressive experimental tests.

The model performance was evaluated against experimental results and it was verified that the ultimate strength, deformation capacity and residual strength of confined concrete were properly captured.

## III. PREDICTIONS BY LITEWKA (2002) MODEL

In this study a model proposed by Litewka et. al. (2002) is compared with experimental results for different loading conditions.

### *A. Theoretical Description [8]*

Mathematical model for deformability of brittle rock-like materials is based on the assumption of tensorial nature of the material damage. The generalized constitutive equations to be presented here consists of the stress strain relations for anisotropic elastic solids

$$\varepsilon_{ij} = A_{ijkl}\sigma_{kl} \qquad (3.1)$$

Where $\varepsilon_{ij}$ is the strain tensor, $\sigma_{kl}$ is the stress tensor and $A_{ijkl}$ is the material constants of orthotropically damaged solid

$$A_{ijkl} = -\frac{v_0}{E_0}\delta_{ij}\delta_{kl} + \frac{1+v_0}{E_0}\left(\delta_{ik}\delta_{jl}+\delta_{il}\delta_{jk}\right) + C\left(\delta_{ij}D_{kl}+D_{ij}\delta_{kl}\right) + D\left(\delta_{ik}D_{jl}+\delta_{jl}D_{ik}+\delta_{jk}D_{il}\right) \qquad (3.2)$$

The above equation contains the Kronecker delta $\delta_{ij}$, the Young modulus $E_0$ and Poisson ratio $\nu_0$ for original undamaged material, two constants $C$ and $D$ to be determined experimentally and the second order symmetric damage effect tensor $D_{ij}$ responsible for current state of internal structure of the material. Substituting the value of $A_{ijkl}$ in the above stress strain relation the following tensor function was obtained.

$$\varepsilon_{ij} = -\frac{v_0}{E_0}\delta_{ij}\sigma_{kk} + \frac{1+v_0}{E_0}\sigma_{ij} + C\left(\delta_{ij}D_{kl}\sigma_{kl}+D_{ij}\sigma_{kk}\right) + 2D\left(\sigma_{ik}D_{kj}+D_{ik}\sigma_{kj}\right) \qquad (3.3)$$

The following non-linear stress strain relations were obtained for uniaxial compression.

$$\varepsilon_1 = \varepsilon_2 = -\frac{v_0}{E_0}\sigma_3 + C\left[\frac{2A{\sigma_3}^3 - 3B{\sigma_3}^3}{3-2A{\sigma_3}^2+3B{\sigma_3}^2} + \frac{2A{\sigma_3}^3}{3-2A{\sigma_3}^2}\right] \qquad (3.4)$$

$$\varepsilon_3 = \frac{\sigma_3}{E_0} + (2C+4D)\left[\frac{2A{\sigma_3}^3 - 3B{\sigma_3}^3}{3-2A{\sigma_3}^2+3B{\sigma_3}^2}\right] \qquad (3.5)$$

Where $\varepsilon_3$ is a longitudinal principal strain and $\varepsilon_1, \varepsilon_2$ are transverse principal strain, A, B, C and D are material constants.

The following non-linear stress strain relations were obtained for biaxial compression.

$$\varepsilon_1 = -\frac{v_0}{E_0}(k+1)\sigma_3 + C\left[\frac{2A(k^2-k+1)(k+1){\sigma_3}^3}{3-2A(k^2-k+1){\sigma_3}^2} + \frac{2A(k^2-k+1)k{\sigma_3}^3+3\sin(\sigma_3)B\sqrt{k^2+1}k^2{\sigma_3}^3}{3-2A(k^2-k+1){\sigma_3}^2-3\sin(\sigma_3)B\sqrt{k^2+1}k{\sigma_3}^3} + \frac{2A(k^2-k+1){\sigma_3}^3+3\sin(\sigma_3)B\sqrt{k^2+1}{\sigma_3}^3}{3-2A(k^2-k+1){\sigma_3}^2-3\sin(\sigma_3)B\sqrt{k^2+1}{\sigma_3}^3}\right] \qquad (3.6)$$

$$\varepsilon_2 = \frac{k-v_0}{E_0}\sigma_3 + C\left[\frac{2A(k^2-k+1){\sigma_3}^3+3\sin(\sigma_3)B\sqrt{k^2+1}{\sigma_3}^3}{3-2A(k^2-k+1){\sigma_3}^2-3\sin(\sigma_3)B\sqrt{k^2+1}{\sigma_3}^3} + (2k+1)\frac{2A(k^2-k+1){\sigma_3}^3+3\sin(\sigma_3)B\sqrt{k^2+1}k{\sigma_3}^3}{3-2A(k^2-k+1){\sigma_3}^2-3\sin(\sigma_3)B\sqrt{k^2+1}k{\sigma_3}^3}\right] + 4D\frac{2A(k^2-k+1)k{\sigma_3}^3+3\sin(\sigma_3)B\sqrt{k^2+1}k^2{\sigma_3}^3}{3-2A(k^2-k+1){\sigma_3}^2-3\sin(\sigma_3)B\sqrt{k^2+1}k{\sigma_3}^3} \qquad (3.7)$$

$$\varepsilon_3 = \frac{1-v_0k}{E_0}\sigma_3 + C\left[\frac{2A(k^2-k+1)k{\sigma_3}^3+3\sin(\sigma_3)B\sqrt{k^2+1}k^2{\sigma_3}^3}{3-2A(k^2-k+1){\sigma_3}^2-3\sin(\sigma_3)B\sqrt{k^2+1}k{\sigma_3}^3} + (k+2)\frac{2A(k^2-k+1){\sigma_3}^3+3\sin(\sigma_3)B\sqrt{k^2+1}{\sigma_3}^3}{3-2A(k^2-k+1){\sigma_3}^2-3\sin(\sigma_3)B\sqrt{k^2+1}{\sigma_3}^3}\right] + 4D\frac{2A(k^2-k+1){\sigma_3}^3+3\sin(\sigma_3)B\sqrt{k^2+1}{\sigma_3}^3}{3-2A(k^2-k+1){\sigma_3}^2-3\sin(\sigma_3)B\sqrt{k^2+1}k{\sigma_3}^3} \qquad (3.8)$$

Where $k = \frac{\sigma_2}{\sigma_3}$

It is mentioned that nineteen standard cubical specimens of the ordinary concrete C20 were uni-axially tested, divided into three groups depending upon the loading. Group1contain four specimens, Group2 contain seven specimens and Group3 contain eight specimens.

The material constants *A*, *B*, *C* and *D* included in the above equation for uniaxial compression case and their respective numerical values together with the other material properties for Group 1, Group 2 and Group 3 of the specimens taken from the experimental work of Liewka are presented in the Table 1.

| Constant | Unit | Group 1 | Group 2 | Group 3 |
|---|---|---|---|---|
| $E_0$ | MPa | 20200 | 19500 | 19500 |
| $V_0$ | - | 0.21 | 0.20 | 0.20 |
| $f_c$ | MPa | -23.9 | -23.9 | -23.9 |
| A | MPa$^{-}$ | 2.244*10^- | 2.255*10^- | 2.150*10^- |

 

| | | | | |
|---|---|---|---|---|
| | $^{2}$ | 3 | 3 | 3 |
| B | $MPa^{-2}$ | 6.174*10^-4 | 6.195*10^-4 | 5.101*10^-4 |
| C | $MPa^{-1}$ | -4.877*10^-6 | -3.508*10^-6 | -1.293*10^-5 |
| D | $MPa^{-1}$ | 1.352*10^-5 | 0.867*10^-5 | 1.778*10^-5 |

Table 1: Material properties and constants for concrete C20 [8]

Figure 3.1 shows normalized stress v/s longitudinal strain curve predicted by the model.

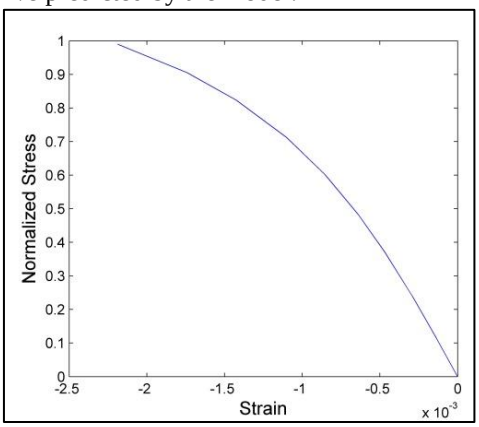


Fig. 3.1: Normalized stress v/s longitudinal strain curve for uniaxial compression.

Figure 3.2 shows normalized stress v/s lateral strain curve predicted by the model.

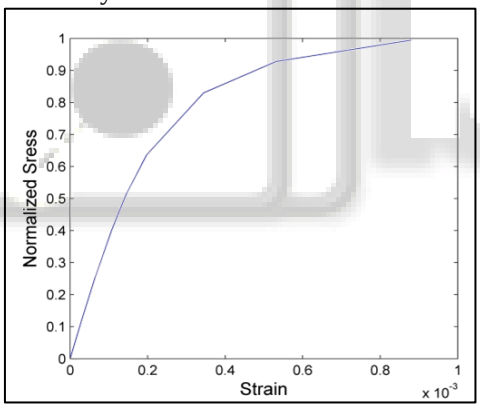


Fig. 3.2: Normalized stress v/s lateral strain curve for uniaxial compression.

The material constants *A*, *B*, *C* and *D* included in the above equation for biaxial compression case and their respective numerical values together with the other material properties for concrete A and concrete B tested by Ligeza are presented in the Table 2.

| Constant | Unit | Concrete A | Concrete B |
|---|---|---|---|
| $E_0$ | MPa | 27900 | 30800 |
| $V_0$ | - | 0.19 | 0.19 |
| $f_c$ | MPa | -14.92 | -28.14 |
| A | $MPa^{-2}$ | 4.432*10^-3 | 1.845*10^-3 |
| B | $MPa^{-2}$ | 3.233*10^-4 | 2.979*10^-4 |
| C | $MPa^{-1}$ | -3.645*10^-6 | -1.457*10^-6 |
| D | $MPa^{-1}$ | 9.338*10^-6 | 6.205*10^-6 |

Table 2: Experimental data and constants for Concrete A and B tested by Ligęza. [8]

Figure 3.3 shows normalized stress v/s longitudinal strain curve predicted by the model.

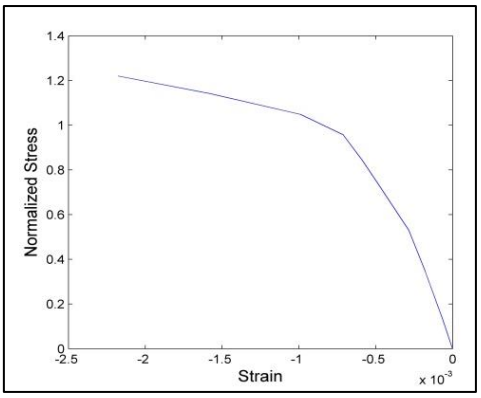


Fig. 3.3: Normalized stress v/s longitudinal strain curve for biaxial compression.

Figure 3.4 shows normalized stress lateral strain curve predicted by the model.

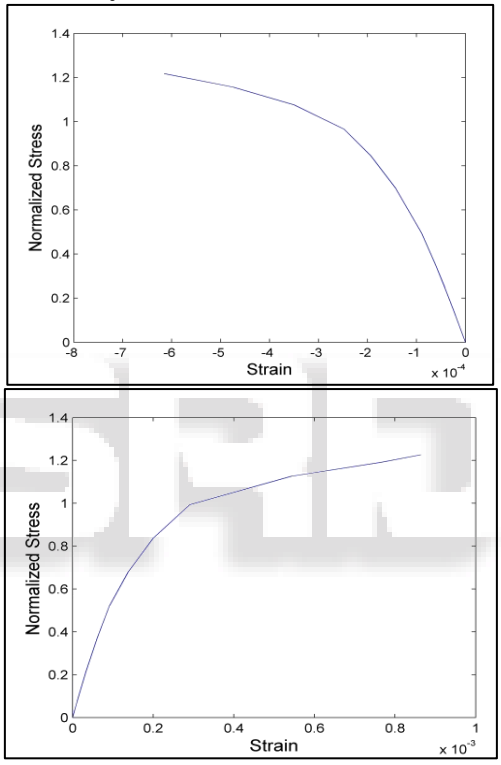


Fig. 3.4: Normalized stress v/s lateral strain curve obtain as for biaxial compression

## IV. RESULTS AND DISCUSSION

Comparison of the stress strain curves for the specimens of Group 1, Group 2 and Group 3 with the experimental results for concrete under uniaxial compression is shown in Figs. 4.1, 4.2 and 4.3.

Fig. 4.1 shows good agreement with experimental for the specimen of Group 1. Moreover, lateral stress-strain behavior is captured well, while the longitudinal strain is moderately overestimated.

Fig. 4.2 shows comparison of predicted results with the experimental results for the specimen of Group 2. The correlation is reasonable for both longitudinal and transverse strain.

Fig. 4.3 shows comparison of predicted results with the experimental results for the specimen of Group 3. Approximately the predicted response is same as that of experiment.

 

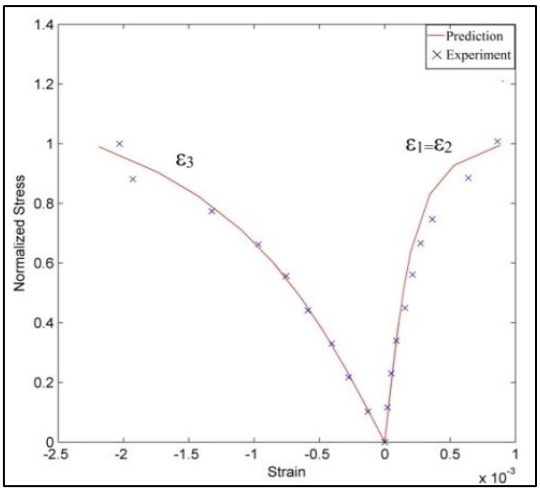


Fig. 4.1: Longitudinal and transverse strain for Group 1 of the specimen v/s longitudinal compressive stress

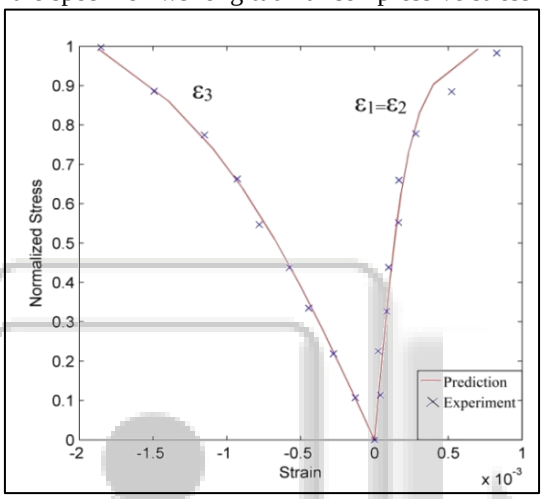


Fig. 4.2: Longitudinal and transverse strain for Group 2 of the specimen v/s longitudinal compressive stress

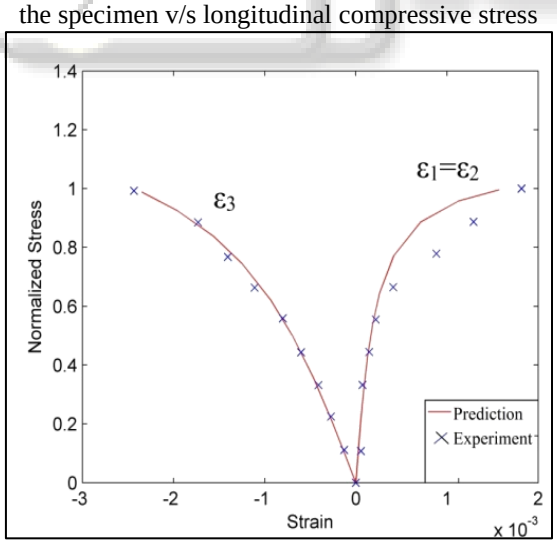


Fig. 4.3: Longitudinal and transverse strain for Group 3 of the specimen v/s longitudinal compressive stress

Verification performed for uniaxial compression of the concrete is not sufficient to evaluate the validity of the simulated model. That is why the more complete analyses of applicability of the simulated model were performed for multi-axial state of stress. Comparison of the stress-strain curves predicted by the model with experimental data for Concrete A and Concrete B tested by Ligęza is shown in Fig. 4.4 and 4.5.

Fig. 4.4 shows comparison of predicted results with the experimental results for concrete A were tested by Ligęza, under biaxial compression for the different values of ratio of the stresses i.e., $k = \sigma 2 / \sigma 3 = 0.5$, $k = 1.0$.

Fig. 4.5 shows comparison of predicted results with the experimental results for concrete B were tested by Ligęza, under biaxial compression for the different values of ratio of the stresses i.e., $k = \sigma 2 / \sigma 3 = 0$, $k = 1.0$. Satisfactory agreement of the predicted and experimental curves seen in Fig. 4.4 and 4.5 corroborate the validity of the simulated model.

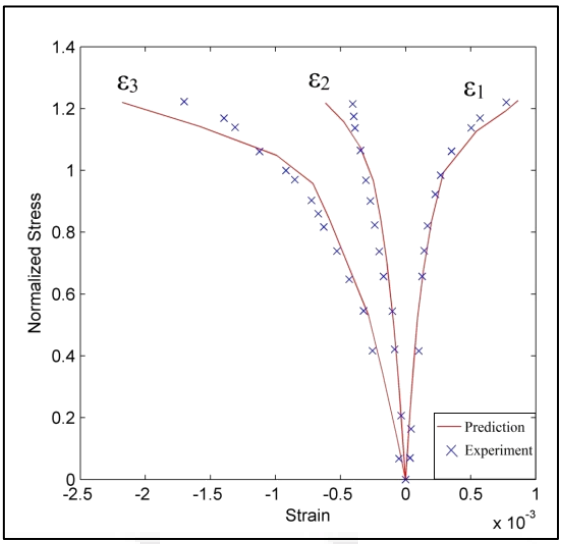


(a)

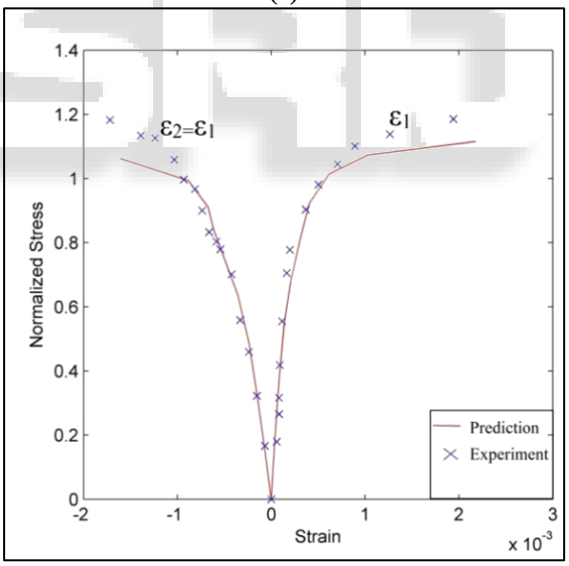


(b)

Fig. 4.4: Stress-strain curves for Concrete A subjected to bi-axial compression:
a) $k = \sigma 2 / \sigma 3 = 0.5$, b) $k = 1.0$

 

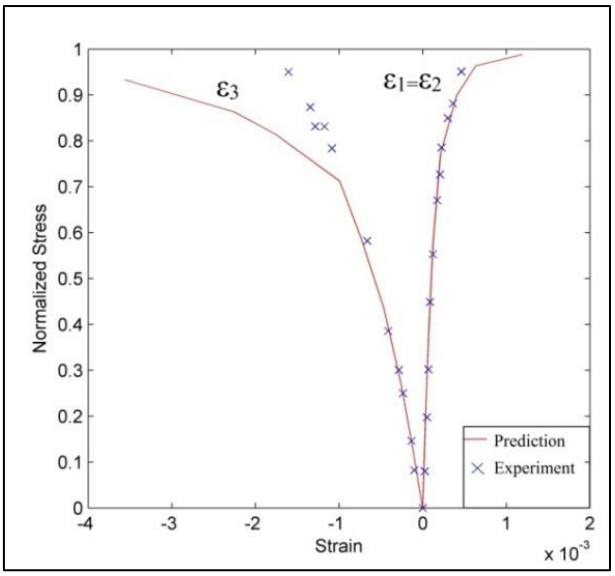


(a)

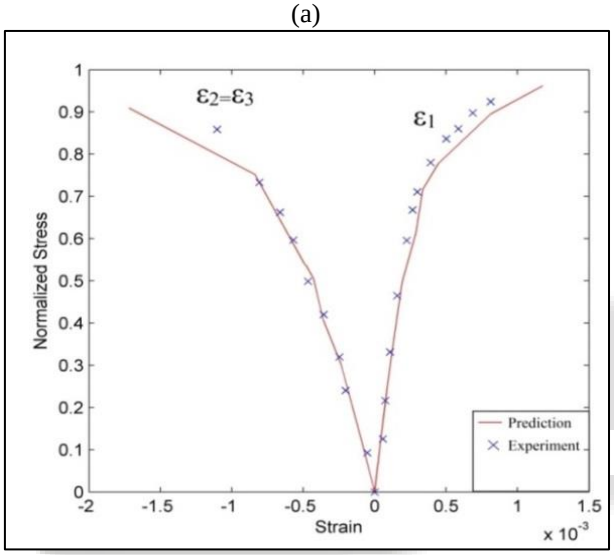


(b)

Fig. 4.5: Stress-strain curves for Concrete B subjected to bi-axial compression: a) $k = \sigma 2 / \sigma 3 = 0$, b) $k = 1.0$

## V. CONCLUSIONS

Based on the study of Litewka et. al. (2002) concrete plasticity model, the following conclusions were drawn:

1) The failure surface serves as a bounding surface, for a plasticity model. It has little or no influence on the deformational behavior of the concrete.
2) Experimental verification of the simulated model performed by employing available experimental data for concrete subjected to multi-axial state of stress showed that predicted stress-strain curves for bi-axial load coincide with experimental data.
3) Predicted stress-strain curves coincide with experimental data. It means that experiments for concrete subjected to uni-axial compression corroborate the validity of the constitutive equations.

## REFERENCES

[1] R. Raveendra Babua, Gurmail S. Benipala and Arbind K. Singhb, "Constitutive modelling of concrete:An overview" Asian journal of civil engineering (building and housing) vol. 6, no. 4 Pages 211-246, 2005.

[2] Willam, K. J., and Warnke, E. P.,(1974) "Constitutive Model for the triaxial behavior of concrete," IABSE Seminar on Concrete Structure Subjected to Triaxial Stresses Paper III-l, Bergamo, Italy, May, 1974.

[3] D.J. Han and W.F. Chen,(1985) "A nonuniform hardening plasticity model for concrete materials" Mechanics of Materials ASCE, 4 (1985) 283-302.

[4] Kupfer, H. Hilsdorf, H.K. and Rush, H. "Behaviour of concrete under biaxial stresses", ACI Journal, 66(1969)656-666.

[5] D.J. Han and W.F. Chen,(1987) "Constitutive modeling in analysis of concrete structures" Journal of Engineering Mechanics, Vol. 113, No. 4, April, 1987. ©ASCE.

[6] Hsuam-Teh Hu and William C. Schnobrich,(1989) "Constitutive modeling of concrete by using nonassociated plasticity" Journal of Materials in Civil Engineering, Vol. 1, No. 4, November, 1989. ©ASCE,

[7] Peter Grassl, Karin Lundgren, Kent Gylltoft,(2002) "Concrete in compression: a plasticity theory with a novel hardening law" International Journal of Solids and Structures 39 (2002) 5205–5223.

[8] Andrzej Litewka, Janina Bogucka, Janusz Dębiński, "Analytical and experimental study of damage induced Anisotropy of concrete", Foundation of civil and environmental engineering. No.02, 2002.

[9] Vassilis K. Papanikolaou, Andreas J. Kappos,(2007) "Confinement-sensitive plasticity constitutive model for concrete in triaxial compression" International Journal of Solids and Structures 44 (2007) 7021–7048.

 